Rietveld refinements of the paraelectric and ferroelectric structures of $PbFe_{0.5}Nb_{0.5}O_3$

1999 J. Phys.: Condens. Matter 11 3489

(http://iopscience.iop.org/0953-8984/11/17/307)

J. Phys.: Condens. Matter **11** (1999) 3489–3500. Printed in the UK PII: S0953-8984(99)95368-7

Rietveld refinements of the paraelectric and ferroelectric structures of $PbFe_{0.5}Nb_{0.5}O_3$

Nathascia Lampis†, Philippe Sciau‡§ and Alessandra Geddo Lehmann†

† Dipartimento di Fisica e INFM, Cittadella Universitaria, Strada Provinciale Monserrato—Sestu km 0.700, 09042-Monserrato (CA), Italy

‡ CEMES-CNRS, 29 rue Jeanne Marvig, BP 4347, 31055 Toulouse Cédex, France

Received 26 July 1998, in final form 2 December 1998

Abstract. The aristotype and the two ettotypes of the complex perovskite $PbFe_{0.5}Nb_{0.5}O_3$ have been refined by the Rietveld method from neutron and x-ray powder diffraction data. To avoid errors due to sample off-stoichiometry or inhomogeneity, only powders obtained by grinding single crystals were analysed. At 523 K the cubic phase (space group $Pm\bar{3}m$), which is known to be stable for $T > 376$ K, has the lattice parameter $a_c = 4.010(1)$ Å and is characterized by disorder of the lead and oxygen atoms, as in most Pb-based complex perovskites. At 363 K the intermediate phase, stable for 355 K $< T <$ 376 K, is confirmed to be tetragonal, space group $P4mm$, with lattice parameters $a_t = 4.007(1)$ Å and $c_t = 4.013(1)$ Å. The best refinement for the low-temperature structure ($T < 355$ K) is obtained, both at 250 and 80 K, in monoclinic symmetry, space group Cm. The monoclinic cell at 250 K has parameters $a_m = 5.674(1)$ Å, $b_m = 5.663(1)$ Å, $c_m = 4.013(1)$ Å and $\beta = 89.84^\circ(2)$.

1. Introduction

There has long been debate about the number and the type of symmetry changes occurring during structural phase transitions in $PbFe_{0.5}Nb_{0.5}O_3$. This compound, which belongs to the wide class of Pb-based complex perovskites with general formula $PbB'_xB''_{1-x}O_3$, was first synthesized as a ceramic by Smolenskii *et al* in 1958 [1] and found to be already ferroelectric at room temperature. The ferroelectric-to-paraelectric transition was located at $T_C \simeq 393$ K [2]. The symmetry of the ferroelectric phase was assessed to be rhombohedral $R3m$ [3, 4]. Rhombohedral lattice parameters were measured in 1970 [5] and the structure refined from powder neutron data in 1984 [6]. According to the previous picture, $PbFe_{0.5}Nb_{0.5}O_3$ was assigned to the ferroic species $m\bar{3}mF3m$, in the Aizu notation [7]—indicating with this symbol the presence of just one ferroelastic/ferroelectric transition from the cubic aristotype to the rhombohedral ettotype.

However, numerous discrepant results appeared after single crystals were synthesized. In a study performed in 1982, Brunskill *et al* [8] found indications of the presence of a second ferroic transition with critical temperature $T_{C2} \simeq 353$ K. The most likely symmetry of the new phase, stable between 353 K and 393 K, was at first suggested to be orthorhombic or monoclinic, on the basis of observations with polarized light microscopy. Diffractometric measurements with high resolution, carried out afterwards on the same crystals by Ehses and Schmid [9], revealed the actual splitting of Bragg reflections between 353 K and 393 K to be tetragonal.

§ Author to whom any correspondence should be addressed.

0953-8984/99/173489+12$19.50

The existence of the second transition in $PbFe_{0.5}Nb_{0.5}O_3$ still remained doubtful very recently. In particular it was not observed in two studies performed on ceramics, i.e. in the aforementioned x-ray and neutron diffraction analysis carried out by Mabud in 1984 [6] and in the x-ray and Mössbauer experiments performed by Darlington in 1991 [10].

As regards the symmetry of the two other accepted phases, Darlington [10] proposed a tetragonal symmetry instead of the rhombohedral one at low temperature, while single-crystal x-ray diffraction performed at 433 K gave an indication of a deviation from the cubic symmetry $Pm\bar{3}m$ well above the quoted Curie point of 393 K, as if a residual distortion were present even in the, in principle, undistorted phase [11].

With the most recent and complete study of the phase transitions in $PbFe_{0.5}Nb_{0.5}O_3$, carried out by Bonny *et al* [12] by single-crystal x-ray diffraction and powder diffraction with synchrotron radiation, all the contradictory literature has merged into a new and consistent picture. Because of the well known difficulties in preparing stoichiometric ceramics of Pb-based perovskites, and because of the proximity of the two phase transitions in $PbFe_{0.5}Nb_{0.5}O_3$, these authors suggested that results could be strongly sample dependent when experiments are performed on powders. Therefore in their study they only used single crystals or powders obtained by grinding them. Their results gave definite confirmation of the existence of the two ferroic transitions joining three phases. The crystal systems of the three phases were determined respectively as monoclinic ($T < 355$ K, ferroic species $m\bar{3}mFm$), tetragonal (355 K $< T <$ 376 K, ferroic species $m\bar{3}mF4mm$) and cubic ($T > 376$ K). The tetragonal phase was assigned to the non-centrosymmetric group $P4mm$ because of its ferroelectric properties. The monoclinic symmetry was indicated as Cm, with a structure based on a diagonal cell with volume twice that of the aristotype.

It is the aim of this paper to present the hitherto lacking refinements of the three structures of $PbFe_{0.5}Nb_{0.5}O_3$. The refinements were performed on neutron and x-ray powder diffraction data.

2. Experimental procedure

2.1. Samples

Single crystals of $PbFe_{0.5}Nb_{0.5}O_3$ were grown in sealed Pt crucibles by the flux method from a high-temperature PbO solution, as described in [8]. The perovskite crystals obtained grew together with a pyrochlore phase of very different colour and morphology. They were easily separated by hand under the microscope and ground into fine powder for preliminary x-ray analysis. The diffraction pattern proved the powder obtained to be free from the secondary phase.

2.2. Data collection and refinement

The neutron experiments were performed at the Laboratoire Leon Brillouin using the Orphée reactor facilities (Saclay, France) on a thermal source. The powder diffraction patterns were collected on the high-resolution two-axis goniometer 3T2 ($\lambda = 1.225$ Å), equipped with a cryofurnace, using steps of 0.05° between 5° and 125° (2θ), $(\sin\theta_{max})/\lambda = 0.72$ Å^{-1}. The measuring temperatures were chosen as $T_1 = 523$ K, $T_2 = 363$ K, $T_3 = 250$ K, with a temperature stability of 0.5 K.

X-ray measurements were performed at 363 K, 250 K and 80 K on a prototype two-axis goniometer (Bragg–Brentano geometry), equipped with a (Cu) rotating-anode generator of 18 kW, at the Laboratoire de Chimie-Physique du Solide of the Ecole Centrale de Paris

(Chatenay-Malabry, France). A cryofurnace was used with about 0.5 K temperature stability. The patterns were scanned using steps from 0.02° to 0.2° between 17° and 155° (2θ). The enhanced intensity of the pseudo-cubic $h00$-type reflections in the preliminary x-ray data collection indicated a strong tendency towards preferential orientation, as already observed for the analogous compound $PbFe_{0.5}Ta_{0.5}O_3$ [13]. In spite of the special care taken in the sample preparation, this problem was not completely eliminated.

Structure refinements were carried out using the profile Rietveld method by means of the program XND [14].

Experimental details are given in table 1.

Table 1. Measurements and refinement conditions.

	X-rays	Neutrons
Data collection		
Diffractometer	Microcontrol	3T2
Monochromator	Graphite	Ge(115)
Instrument geometry	Bragg–Brentano	Transmission
Temperature (K)	363, 250, 80	523, 363, 250
Radiation	Cu Kβ	
Wavelength (Å)	1.39217	1.225
Step (2θ)/x-ray time; range (2θ)	0.02°/10 s; 17°–57°, 0.04°/40 s; 57°–87°, 0.12°/80 s; 87°–110°, 0.20°/120 s; 110°–155°	0.05°; 5°–125°
$(\sin\theta)/\lambda_{max}$ (Å^{-1})	0.70	0.72
Number of points	3160	2400
Refinements		
	Refinement on	$S = \sum w_i(Y_{oi} - Y_{ci})^2$
	Weighting scheme	$w_i = 1/Y_{oi}$
	Analytical function for profile	Pseudo-Voigt
	R-factors	$R_{wp} = \{[\sum w_i(Y_{oi} - Y_{ci})^2]/[\sum w_i(Y_{oi})]\}^{1/2}$ $R_B = (\sum \lvert I_{oK} - I_{cK}\rvert)/\sum I_{oK}$ GoF $= [S/(N-P)]^{1/2}$ R_{wp_c} = modified R_{wp} taking into account the local correlations [15]
	Program for refinement	XND 1.11 [14]

3. Results

3.1. Structure at 523 K

The ideal cubic perovskite (space group $Pm\bar{3}m$) was taken as the starting model for the cubic refinement of the neutron diffraction patterns. The atoms were at first fixed at their special Wyckoff positions. With this choice, the refined thermal motion parameter of Pb was abnormally large ($B_{\mathrm{Pb}} = 3.68(3)$ Å^2), indicating the likely presence of structural disorder.

Structural disorder is a common feature of most Pb-based complex perovskites, a class of compounds in which the ideal perovskite structure, in spite of its apparent simplicity, seems never to be realized. Structure refinements, performed either on powders or on single crystals, have been published for the aristotypes of the following compounds: Pb_2CoWO_6

[16], Pb_2MgTeO_6 [17], Pb_2MgWO_6 [18], $PbSc_{0.5}(Ti_{0.25}Te_{0.25})O_6$ [19], $PbFe_{0.5}Ta_{0.5}O_3$ [13], Pb_2ScTaO_6 [20], $PbSc_{0.5}Nb_{0.5}O_3$ [21] and $PbMg_{0.33}Nb_{0.67}O_6$ [20, 22]. All of these examples are characterized by a high degree of positional disorder, either at cationic or at anionic sites or at both, as a common structural feature. With reference to cationic disorder, Pb is never found at its ideal Wyckoff position, being instead statistically split over several sites around it. Split positions for B′ and B″ have a much less pronounced effect on the refinement owing to the small value of the displacement from the special position. The treatment of oxygen atoms is the most subtle: the refined thermal motions are not only large but also strongly anisotropic. Their large size has been sometimes interpreted as disorder (either static or dynamic), and structural models with split oxygen sites have been proposed [16, 21]. In contrast, it has been remarked [21] that the strong anisotropy could not be modelled by simple static shifts and that anharmonic treatments should be performed in a better way.

Therefore in the next stage of our refinement, Pb was supposed to be located in a multi-minima potential around its special Wyckoff position. Three possible kinds of Pb disorder were considered: along ⟨100⟩, ⟨110⟩ and ⟨111⟩ directions.

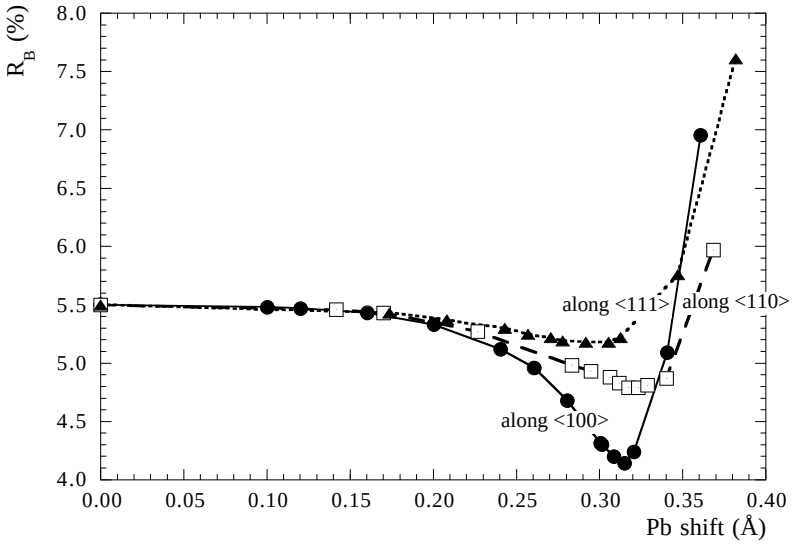

Figure 1. R_B versus the Pb shift for the cubic phase of $PbFe_{0.5}Nb_{0.5}O_3$. The $\langle 100\rangle_{Pb}$ model shows the deepest R_B-minimum.

Figure 1 shows the agreement coefficient R_B plotted as a function of the Pb shift from the ideal position for the three kinds of disorder. This figure was obtained by varying step by step the position of Pb and refining all of the other parameters. Oxygen was treated anisotropically. The $\langle 100\rangle_{Pb}$ model has the deepest R_B-minimum, with one Pb atom statistically disposed at 6e Wyckoff positions at a distance of 0.315 Å from the ideal position. However, this result must be treated with great caution. In fact, as already stressed [23], a direction of displacement can appear preferred with respect to others just as a consequence of a too small value of $(\sin\theta)/\lambda$. For this reason, for other compounds [20] the positions occupied by Pb have been described as distributed over a sphere.

The cubic structural parameters are reported in table 2. As can be seen, the thermal ellipsoid of oxygen is strongly anisotropic, with vibrations occurring mainly within the faces of the cubic cell. In spite of the large anisotropy, a model with oxygen in a harmonic multi-

Table 2. Structural parameters at 523 K. Space group $Pm\bar{3}m$; $a = 4.010(1)$ Å, $R_{wp} = 7.37\%$, $R_B = 4.17\%$. Δx: the Pb shift from the special position of the ideal cubic perovskite. $B_{eq} = (4/3)\sum\sum\beta_{ij}\vec{a}_i \cdot \vec{a}_j$. Number of refined parameters: 27. NB The refinement was with O isotropic and disordered at 12h sites: $a = 4.0104(7)$ Å, $R_{wp} = 7.35\%$, $R_B = 3.92\%$. $\Delta x_{\mathrm{Pb}} = 0.314(1)$ Å, $\Delta x_{\mathrm{O}} = 0.179(2)$ Å, B_{iso}(Pb) $= 0.60(3)$ Å^2, B_{iso}(Fe/Nb) $= 0.70(2)$ Å^2, B_{iso}(O) $= 0.41(2)$ Å^2. Number of refined parameters: 26.

Atom	x	y	z	B_{eq} (Å^2)	β_{11}	β_{22}	β_{33}	Δx (Å)
Fe/Nb at 1b	0.5	0.5	0.5	0.71(2)				
Pb at 6e	0.0783(3)	0	0	0.60(3)				0.314(1)
O at 3c	0.5	0.5	0	1.31	0.0286(5)	0.0286(5)	0.0040(6)	

minima potential has been tested for the sake of comparison. Disorder along ⟨100⟩ and ⟨110⟩ was tested. All of the thermal motions were refined isotropically. The best refinement was obtained with oxygen split at 12h positions, as reported in the caption of table 2. As can be noted, a weak gain was achieved at the level of the agreement factors. However, in our opinion the quite small numerical improvement is not significant, so the less disordered model should be preferred.

3.2. Structure at 363 K

Neutron and x-ray data for the intermediate phase were refined in the tetragonal space group $P4mm$ proposed by Bonny *et al* [12]. The cubic model of symmetry $Pm\bar{3}m$ was also tested for comparison.

In the neutron refinements, the atoms were at first fixed at their special positions in the tetragonal $P4mm$ and cubic $Pm\bar{3}m$ symmetries. The atomic thermal motions were refined isotropically (models T1 and C1, respectively, for tetragonal and cubic). For each of the two symmetries, the final thermal parameter of Pb was abnormally large (3.64(1) Å^2 and 3.54(3) Å^2 respectively). A better agreement was obtained with model T1 (cf. table 3), confirming the tetragonal symmetry.

Table 3. Results of the neutron data refinement at 363 K. Models: C1 ($Pm\bar{3}m$): ordered, all thermal motions isotropic; T1 ($P4mm$): ordered, all thermal motions isotropic; T2 ($P4mm$): ordered, anisotropic thermal motions for Pb and O.

	R_{wp} (%)	R_{wp_c} (%)	R_B (%)	GoF	No of parameters
Model C1	8.20	14.13	6.63	1.34	26
Model T1	7.41	11.11	4.81	1.21	32
Model T2	7.19	10.09	4.16	1.17	36

In the second step, both Pb and O were refined anisotropically (model T2). This led to a further improvement in the agreement coefficients (cf. table 3).

At this stage of the analysis we focused our attention on the thermal ellipsoids of oxygen and lead. The thermal ellipsoids of oxygen atoms were strongly anisotropic, leading to vibrations occurring mainly perpendicular to the oxygen–Fe/Nb bonds, as in the cubic phase at 523 K. In contrast, the thermal ellipsoid of Pb converged to a sphere with an equivalent thermal factor $B_{eq} = 3.54$ Å^2 comparable to the isotropic one (3.64(1) Å^2) and to the value found at 523 K in the cubic phase before the introduction of positional disorder (3.68(3) Å^2). This result indicates that Pb disorder is present in the tetragonal phase too, with an almost isotropic distribution around the special position, as shown by the spherical symmetry of the thermal

ellipsoid. Attempts at finding the disordered tetragonal model failed because of the strong correlation among the free parameters during refinement. Given the difficulty of specifying the direction of the Pb displacements, the structural parameters for the tetragonal structure reported in table 4 refer to model T2.

Table 4. Final structural parameters at 363 K. Space group $P4mm$; $a = 4.007(1)$ Å, $c = 4.013(1)$ Å ($R_{wp} = 7.19\%$, $R_B = 4.16\%$). The oxygen thermal displacements are mainly perpendicular to the Fe/Nb–O bonds. $B_{eq} = (4/3)\sum\sum \beta_{ij}\vec{a}_i \cdot \vec{a}_j$.

Atom	x	y	z	B_{eq} (Å^2)	β_{11}	β_{22}	β_{33}
Fe/Nb at 1b	0.5	0.5	0.5	0.60(4)			
Pb at 1a	0	0	0.004(8)	3.54	0.054(2)	0.054(2)	0.057(3)
O1 at 1b	0.5	0.5	0.030(5)	1.03	0.023(4)	0.023(4)	0.002(4)
O2 at 2c	0.5	0	0.492(3)	1.15	0.023(5)	0.002(1)	0.030(5)

X-ray data were refined in the cubic (C1) and tetragonal (T1) models obtained from neutron data. The tetragonal model gave an improvement of the R_{wp}-factor (7.19%, compared with 8.62% for the cubic model) but not of the R_B-factor (5.63%, compared with 5.73% for the cubic model). The reason for the poor R_B-factor improvement is found by analysing the difference between the cubic and the tetragonal phases: as can be seen, it mainly concerns oxygen atoms. As is well known, x-rays are less sensitive than neutrons to oxygen. In contrast, the difference between the two R_{wp}-factors is relevant, on account of the fact that the tetragonal distortion is more evident in the x-ray pattern than in the neutron pattern because of the higher resolution.

In both models, preferential orientation correction was necessary along the $\langle 100\rangle_{cub}$ directions. This correction gave a good fitting for $h00$-type and $hh0$-type reflections, while hhh-type ones were systematically underestimated.

3.3. Structure at 250 K and 80 K

Neutron (at 250 K) and x-ray (at 250 K and 80 K) data were analysed. Taking into consideration the debate found in the literature, the data were refined both in the recently proposed monoclinic model [12] and in the usually assumed rhombohedral structure.

For the two models the cubic positions were used as initial ones. We used isotropic thermal factors for O and Fe/Nb, while Pb was treated anisotropically. In the case of the x-ray data, the oxygen thermal factor was fixed and not refined. The same procedure was adopted for Fe/Nb at 80 K, because a negative value was obtained when the thermal parameter was refined.

Table 5. Results of the neutron data refinement at 250 K.

	R_{wp} (%)	R_{wp_c} (%)	R_B (%)	GoF	No of parameters
Monoclinic model	7.30	10.93	3.67	1.21	41
Rhombohedral model	7.43	11.79	4.27	1.23	32

The monoclinic model gives the best result for both sets of data, as shown in table 5 and table 6. The gain obtained with the monoclinic structure is more evident at 80 K, when the monoclinic distortion is stronger. At this temperature the gain in R_B is of 2.4%, i.e. even more important than the one obtained for the tetragonal model T1 with respect to the cubic one C1 at 363 K.

The Rietveld refinement of the neutron pattern at 250 K in monoclinic symmetry is shown in figure 2.

Table 6. Results of the x-ray data refinement at 250 K and 80 K.

		R_{wp} (%)	R_{wp_c} (%)	R_B (%)	GoF	No of parameters
Monoclinic model	250 K	7.64	17.79	5.51	1.96	49
	80 K	8.39	21.84	6.37	2.23	48
Rhombohedral model	250 K	8.06	19.92	5.35	2.06	41
	80 K	10.31	31.72	8.81	2.73	40

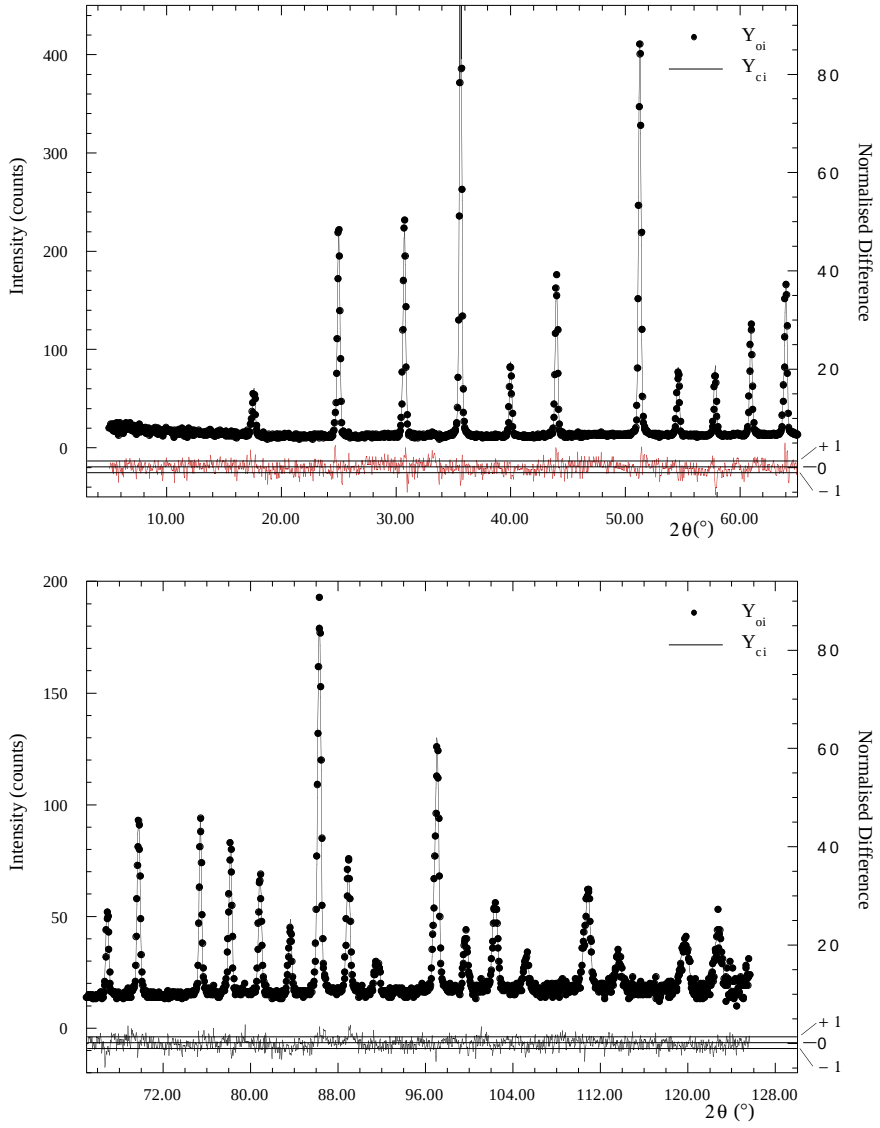

Figure 2. The Rietveld refinement of the neutron diffraction pattern at $T = 250$ K, showing the experimental and the calculated profile. The normalized difference curve $\Delta_{norm} = (Y_{oi} - Y_{ci})/\sigma(Y_{oi})$ is plotted at the bottom. Tick lines corresponding to $\Delta_{norm} = \pm 1$ are indicated.

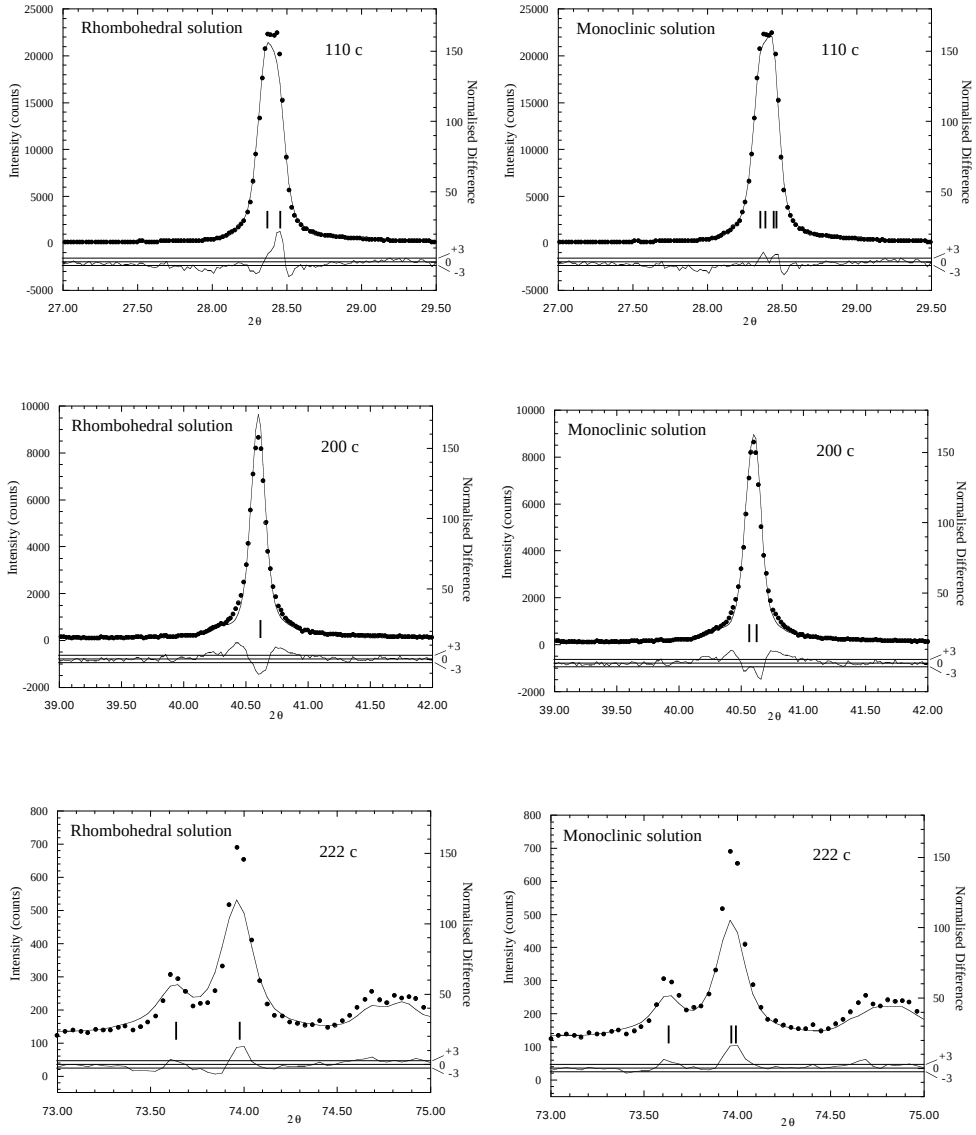

Figure 3. Details of the Rietveld refinement of the x-ray pattern at $T = 80$ K. Left-hand panels: rhombohedral model. Right-hand panels: monoclinic model. Experimental (points) and calculated (curve) profiles are shown. The normalized difference curve Δ_{norm} is plotted at the bottom. Tick lines corresponding to $\Delta_{norm} = \pm 3$ are indicated. The reflections $(110)_{cub}$ and $(200)_{cub}$ are better reproduced in the monoclinic model. The reflection $(222)_{cub}$ appears not to be well fitted in both models, owing to the preferential orientation not being completely reproduced in the calculated profile.

The refined x-ray profiles at 80 K in the two symmetries are shown in figure 3 for selected reflections. As can be seen, the observed pattern is better reproduced as monoclinic for reflections of the type $(hh0)_{cub}$ and $(h00)_{cub}$. As already found in tetragonal symmetry, the experimental intensities of the reflections $(hhh)_{cub}$ are underestimated in both models because of the difficulty in modelling preferential orientation after ferroelastic transitions.

Table 7. Final structural parameters for the monoclinic model at 250 K and 80 K. Space group Cm.

		250 K		80 K
		Neutrons	X-ray	X-ray
Fe/Nb	x	0.483(5)	0.480(5)	0.477(2)
	y	0	0	0
	z	0.479(6)	0.474(6)	0.474(3)
	B_{iso}	0.66(5)	0.5(1)	0.15
Pb	x	0	0	0
	y	0	0	0
	z	0	0	0
	B_{eq}	2.75	2.72	2.64
	β_{11}	0.017(4)	0.018(3)	0.017(2)
	β_{22}	0.025(4)	0.024(3)	0.030(1)
	β_{33}	0.043(8)	0.042(4)	0.029(2)
	β_{13}	−0.017(6)	−0.013(6)	−0.013(3)
O1	x	0.488(4)	0.46(2)	0.46(1)
	y	0	0	0
	z	−0.019(8)	−0.03(2)	−0.07(1)
	B_{iso}	0.7(2)	0.6	0.2
O2	x	0.213(3)	0.21(1)	0.213(9)
	y	0.235(1)	0.245(8)	0.248(7)
	z	0.450(5)	0.44(1)	0.45(1)
	B_{iso}	0.48(8)	0.6	0.2
	a (Å)	5.674(1)	5.676(1)	5.678(1)
	b (Å)	5.663(1)	5.668(1)	5.663(1)
	c (Å)	4.013(1)	4.015(1)	4.016(1)
	β	89.84°(2)	89.84°(2)	89.75°(3)

Monoclinic structural parameters are given in table 7. Results from neutron and x-ray data agree within the estimated errors. In both the rhombohedral and the monoclinic refinements the thermal ellipsoid of Pb was found to be large and strongly anisotropic. In particular, the anisotropic character of Pb is much more pronounced than in the intermediate tetragonal phase. Such a large thermal ellipsoid at a temperature of 80 K might in principle be a sign of disorder or of incorrect symmetry assignment. As no additional reflection is present either in the neutron or in the x-ray patterns, the possibility of the existence of a superstructure can be rejected. Triclinic symmetry has been tested, with no improvement in spite of the greater number of refined parameters. Moreover, the B-factor of Pb remained large. In conclusion, Pb is disordered and the symmetry is pseudo-rhombohedral, with a small monoclinic distortion. The thermal ellipsoid is flattened along the pseudo-ternary axis ($U_1 = 0.012$ Å^2) and spread in the normal plane ($U_2 = 0.041$ Å^2, $U_3 = 0.051$ Å^2)

4. Concluding remarks

The structural modifications induced in $PbFe_{0.5}Nb_{0.}O_3$ at each phase transition are displayed in figure 4. At the cubic-to-tetragonal transition the ferroelastic strain is very weak ($c/a = 1.01$). The Fe/Nb–oxygen octahedron is slightly distorted. The axial oxygen atom O1 is shifted along

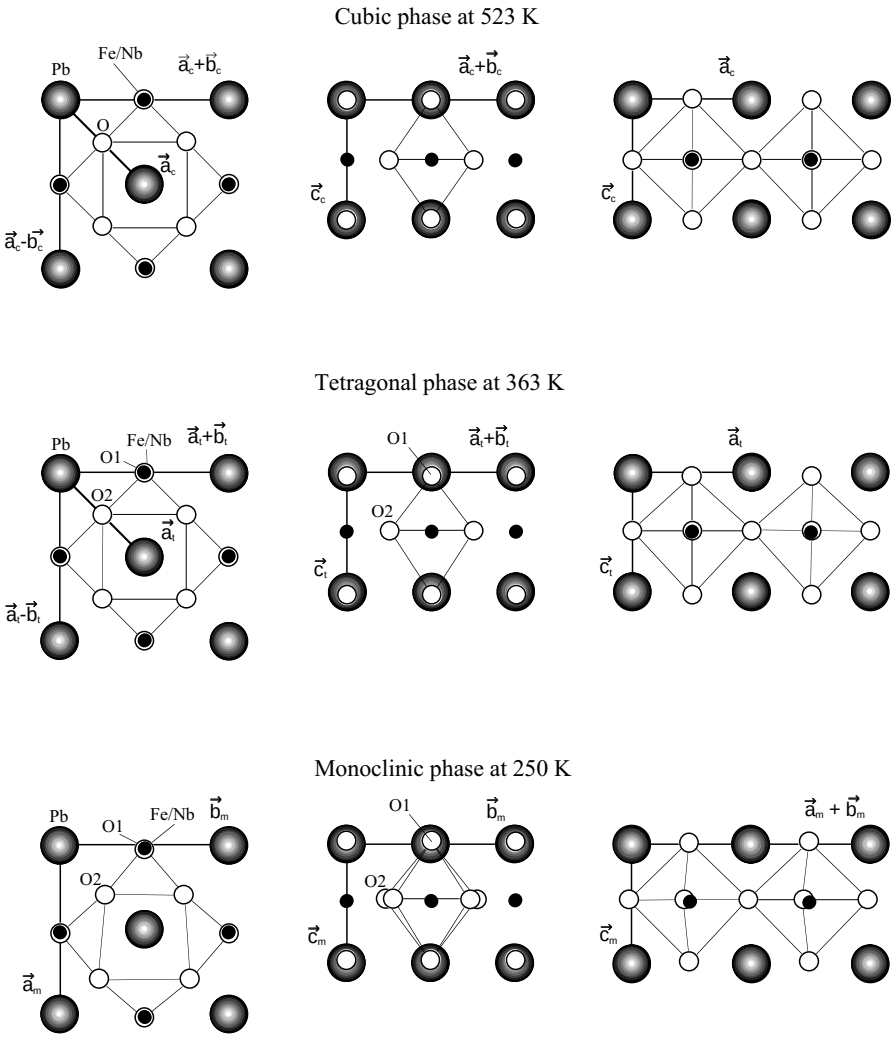

Figure 4. Structural modifications in $PbFe_{0.5}Nb_{0.5}O_3$ at the phase transitions. Different projections are displayed for the three (cubic, tetragonal, monoclinic) phases.

the unique fourfold axis towards Fe/Nb by 0.12(2) Å and the planar oxygen O2 is shifted along the same direction by −0.03(1) Å. The displacement of Pb is not significant (−0.02(3) Å). Oxygen shifts produce three different O–O bond lengths, as can be seen from table 8. As a result, Fe/Nb is not located at the centre of the octahedron, while Pb is almost at the centre of the cuboctahedron. The electric polarization is mainly due to the relative displacements of oxygen and Fe/Nb.

The main structural modifications at the tetragonal-to-monoclinic transition consist in large shifts of O atoms: O1 is shifted approximately along $[-1\ -1\ -2]_t$ and O2 along $[-1\ -2\ -1]_t$ tetragonal directions. Fe/Nb is displaced approximately along the $[-1\,-1\,-1]_t$ (or [111] cubic direction). The resulting monoclinic distortion is very weak and the symmetry is pseudo-rhombohedral. As can be seen from table 8, Fe/Nb is not far from the centre of the octahedra, while Pb is well away from the centre of the cuboctahedra. The small Pb–O distance

Table 8. Bond distances (Å) at 523 K, 363 K and 250 K obtained from neutron refinements. In the cubic phase, the disorder of Pb and O atoms was not considered.

Distance	Cubic	Tetragonal	Monoclinic
Fe/Nb–O	2.005(1) × 6	1.89(4) × 1	1.99(2) × 2
		2.004(1) × 4	2.00(4) × 1
		2.13(4) × 1	2.01(4) × 1
			2.03(1) × 2
Pb–O	2.836(1) × 12	2.801(8) × 4	2.55(2) × 2
		2.835(1) × 4	2.77(2) × 1
		2.870(9) × 4	2.833(1) × 2
			2.84(2) × 2
			2.85(2) × 2
			2.91(2) × 1
			3.13(2) × 2
O–O	2.836(1) × 12	2.73(2) × 4	2.66(1) × 1
		2.833(1) × 4	2.73(3) × 2
		2.94(2) × 4	2.78(3) × 2
			2.842(1) × 2
			2.90(3) × 2
			2.96(3) × 2
			3.00(1) × 1

changes from 2.81 Å (tetragonal) to 2.56 Å (monoclinic). Therefore in the monoclinic phase the electric polarization is strengthened owing to the relative displacement of O and Pb.

The structure of $PbFe_{0.5}Nb_{0.5}O_3$ is characterized by a high degree of Pb positional disorder, which appears to be present over a wide range of temperature. Pb is disordered in the cubic phase and its displacement with respect to the ideal position is slightly larger than in other similar perovskites, for example $PbFe_{0.5}Ta_{0.5}O_3$ [13], $PbSc_{0.5}Nb_{0.5}O_3$ [21] and Pb_2ScTaO_6 [20]. With lowering temperature and passage through the sequence of phase transitions, the thermal parameter of Pb remains large, never attaining a normal value. In this sense, Pb appears to remain disordered even at 80 K. A similar result is found for rhombohedral $PbSc_{0.5}Nb_{0.5}O_3$ [21] and Pb_2MgTeO_6 [17] and for pseudo-rhombohedral $PbFe_{0.5}Ta_{0.5}O_3$ [24].

As regards the structural features related to Pb, there seems therefore to be a difference between Pb-based perovskites, the main distortion of which is rhombohedral, and those in which this distortion is tetragonal. In these latter no disorder is present at low temperature. Well known examples are Pb_2MgWO_6 [18] and $PbTiO_3$ [20, 25], in which the thermal ellipsoid of Pb, large at high temperature, attains a normal value below the phase transition. It has been suggested [26] that one reason for the adoption of split positions of Pb can be its tendency to form PbO_4 coordination polyhedra, in the presence of which the whole structural stability is enhanced, as found for $PbTiO_3$ [27]. This coordination polyhedron has been found in the pseudo-tetragonal low-temperature phase of Pb_2MgWO_6. This structural layout can be realized at least locally in rhombohedral symmetry if Pb moves away from the ternary axis and splits over several sites around it. In contrast, an ordered configuration with Pb in a special position on the threefold axis would allow only the PbO_3 coordination.

A different behaviour characterizes oxygen atoms. In fact the oxygen Debye–Waller factor decreases on lowering the temperature and attains a normal value in the monoclinic phase. A point of interest is the strong anisotropy of oxygen thermal ellipsoids. In the cubic phase it is $\beta_{11}(\mathrm{O}) = \beta_{22}(\mathrm{O}) \approx 6\beta_{33}(\mathrm{O})$; in the tetragonal phase $\beta_{11}(\mathrm{O1}) = \beta_{22}(\mathrm{O1}) \approx 10\beta_{33}(\mathrm{O1})$ and

$\beta_{11}(O2) \approx \beta_{33}(O2) \approx 10\beta_{22}(O2)$. Such anisotropy has already been observed in perovskites and has been associated with low-frequency rotation modes of oxygen octahedra [28–30] that can condense to produce complex superstructure at lower temperature. However, in the case of $PbFe_{0.5}Nb_{0.5}O_3$ the low-temperature monoclinic cell does not correspond to the freezing of such zone-boundary modes, as proved by the absence of superstructure reflections.

A final remark can be made which concerns the absence of relaxor properties for $PbFe_{0.5}Nb_{0.5}O_3$. It is known in fact that the dielectric susceptibility of this compound has no frequency dependence, in spite of the presence of both random B- and B′-species distributions and Pb disorder, which are the two structural features currently thought to be responsible for relaxor behaviour. In particular, the disorder of Pb leads to a local polarization which is different from the macroscopic one. It is well known that in the case of non-vanishing intercell correlation a connection exists between the local polarization in neighbouring cells and relaxor properties. Therefore in $PbFe_{0.5}Nb_{0.5}O_3$ the intercell correlation must be weak, in particular at least weaker than in the relaxor $PbSc_{0.5}Nb_{0.5}O_3$, and in any case not sufficient to cause the formation of polar nanodomains of correlated cells.

References

[1] Smolenskii G A, Agranovskaia A I, Popov S N and Isupov V A 1958 *Sov. Phys.–Tech. Phys.* **3** 1981
[2] Smolenskii G A and Bokov V A 1964 *J. Appl. Phys.* **35** 915
[3] Platonov G L, Tomashpol'skii Yu Ya, Venevtsev Yu N and Zhdanov G S 1967 *Bull. Acad. Sci. USSR, Phys. Ser.* **31** 1108
[4] Astrov D N, Al'schin B I, Zorin R V and Drobyshev 1969 *Sov. Phys.–JETP* **28** 1123
[5] Platonov G L, Drobyshev L A, Tomashpol'skii Yu Ya and Venevtsev Yu N 1970 *Sov. Phys.–Crystallogr.* **14** 692
[6] Mabud S A 1984 *Phase Transitions* **4** 183
[7] Aizu K 1970 *Phys. Rev.* B **2** 754
[8] Brunskill I H, Boutellier R, Depmeier W, Schmid H and Scheel H J 1982 *J. Cryst. Growth* **56** 541
[9] Ehses K H and Schmid H 1993 *Z. Kristallogr.* **162** 64
[10] Darlington C N W 1991 *J. Phys.: Condens. Matter* **3** 4173
[11] Kolesova R and Kupriyanov M 1993 *Phase Transitions* **45** 271
[12] Bonny V, Bonin M, Sciau Ph, Schenk K J and Chapuis G 1997 *Solid State Commun.* **102** 347
[13] Geddo Lehmann A, Kubel F and Schmid H 1997 *J. Phys.: Condens. Matter* **9** 8201
[14] Bérar J F and Garnier P 1992 *APD 2nd Conf. (NIST Special Publication 846)* (Washington, DC: US Government Printing Office) p 212
XND is available by anonymous ftp at ftp://labs.polycnrs-gre.fr/pub/xnd
[15] Bérar J F and Lelann P 1991 *J. Appl. Crystallogr.* **24** 1
[16] Baldinozzi G, Sciau Ph and Lapasset J 1992 *Phys. Status Solidi* a **133** 17
[17] Baldinozzi G, Grebille D, Sciau Ph, Kiat J M, Moret J and Bérar J F 1998 *J. Phys.: Condens. Matter* **10** 6461
[18] Baldinozzi G, Sciau Ph, Pinot M and Grebille D 1995 *Acta Crystallogr.* B **51** 668
[19] Alonso J A and Rasines I 1988 *J. Phys. Chem. Solids* **49** 385
[20] Zhukov S G, Chernyshev V V, Aslanov L A, Vakhrushev S B and Schenk H 1995 *J. Appl. Crystallogr.* **28** 385
[21] Malibert C, Dkhil B, Kiat J M, Durand D, Bérar J F and Spasojevic-de Biré A 1997 *J. Phys.: Condens. Matter* **9** 7485
[22] Verbaere A, Piffard Y, Yé Z G and Husson E 1992 *Mater. Res. Bull.* **27** 1927
[23] Vakhrushev S, Zhukov S, Fetisov G and Chernyshov V 1994 *J. Phys.: Condens. Matter* **6** 4021
[24] Lampis N, Sciau Ph and Geddo Lehmann A 1999 *J. Phys.: Condens. Matter* at press
[25] Nelmes R J, Piltz R O, Kuhs W F, Tun Z and Restori R 1985 *Ferroelectrics* **93** 379
[26] Rivezzi N and Sciau Ph 1998 *J. Solid State Chem.* **139** 332
[27] Cohen R E 1992 *Nature* **358** 136
[28] Hewat A W 1973 *J. Phys. C: Solid State Phys.* **6** 2559
[29] Hewat A W 1972 *Phys. Status Solidi* b **53** K33
[30] Glazer A and Megaw H D 1972 *Phil. Mag.* **25** 1119